



<b>Publication Year</b>	2016
<b>Acceptance in OA @INAF</b>	2021-04-16T09:40:26Z
<b>Title</b>	Artifacts reduction in VIR/Dawn data
<b>Authors</b>	CARROZZO, FILIPPO GIACOMO; RAPONI, Andrea; DE SANCTIS, MARIA CRISTINA; Ammannito, E.; Giardino, M.; et al.
<b>DOI</b>	10.1063/1.4972256
<b>Handle</b>	<a href="http://hdl.handle.net/20.500.12386/30769">http://hdl.handle.net/20.500.12386/30769</a>
<b>Journal</b>	REVIEW OF SCIENTIFIC INSTRUMENTS
<b>Number</b>	87

## Artifacts reduction in VIR/Dawn data

F. G. Carrozzo, A. Raponi, M. C. De Sanctis, E. Ammannito, M. Giardino, E. D'Aversa, S. Fonte, and F. Tosi

Citation: *Rev. Sci. Instrum.* **87**, 124501 (2016); doi: 10.1063/1.4972256

View online: <http://dx.doi.org/10.1063/1.4972256>

View Table of Contents: <http://aip.scitation.org/toc/rsi/87/12>

Published by the [American Institute of Physics](#)

---

---

## Artifacts reduction in VIR/Dawn data

F. G. Carrozzo,<sup>1,a)</sup> A. Raponi,<sup>1</sup> M. C. De Sanctis,<sup>1</sup> E. Ammannito,<sup>2</sup> M. Giardino,<sup>1</sup>  
 E. D'Aversa,<sup>1</sup> S. Fonte,<sup>1</sup> and F. Tosi<sup>1</sup>

<sup>1</sup>*Istituto di Astrofisica e Planetologia Spaziali-Istituto Nazionale di Astrofisica, Via Fosso del Cavaliere 100,  
 00133 Rome, Italy*

<sup>2</sup>*Institute of Geophysics and Planetary Physics, University of California Los Angeles, 595 Charles Young Drive  
 East, Los Angeles, California 90095-1567, USA*

(Received 23 June 2016; accepted 1 December 2016; published online 19 December 2016)

Remote sensing images are generally affected by different types of noise that degrade the quality of the spectral data (i.e., stripes and spikes). Hyperspectral images returned by a Visible and InfraRed (VIR) spectrometer onboard the NASA Dawn mission exhibit residual systematic artifacts. VIR is an imaging spectrometer coupling high spectral and spatial resolutions in the visible and infrared spectral domain (0.25–5.0  $\mu\text{m}$ ). VIR data present one type of noise that may mask or distort real features (i.e., spikes and stripes), which may lead to misinterpretation of the surface composition. This paper presents a technique for the minimization of artifacts in VIR data that include a new instrument response function combining ground and in-flight radiometric measurements, correction of spectral spikes, odd-even band effects, systematic vertical stripes, high-frequency noise, and comparison with ground telescopic spectra of Vesta and Ceres. We developed a correction of artifacts in a two steps process: creation of the artifacts matrix and application of the same matrix to the VIR dataset. In the approach presented here, a polynomial function is used to fit the high frequency variations. After applying these corrections, the resulting spectra show improvements of the quality of the data. The new calibrated data enhance the significance of results from the spectral analysis of Vesta and Ceres. *Published by AIP Publishing.* [<http://dx.doi.org/10.1063/1.4972256>]

### I. INTRODUCTION

The Dawn mission to Vesta and Ceres was launched in September 2007 with a scheduled arrival in 2011 at Vesta and in 2015 at Ceres. Dawn's goal is to orbit 4 Vesta and 1 Ceres to obtain measurements in order to better understand the conditions and processes acting during the earliest epoch of the solar system.<sup>1,2</sup>

The instruments onboard Dawn are designed to characterize and map the surface composition of Vesta and Ceres in different radiation ranges that are sensitive to the molecular and elemental chemistry and some physical properties. These include a Framing Camera (FC) with multispectral capabilities, a Visible and InfraRed (VIR) mapping spectrometer, and a Gamma-Ray and Neutron Detector (GRaND).

VIR is a hyperspectral imaging spectrometer (Fig. 1) that acquires hyperspectral images in the overall spectral range from the near ultraviolet (0.25  $\mu\text{m}$ ) to the thermal infrared (5.1  $\mu\text{m}$ ), coupling high spectral and spatial resolutions.<sup>3</sup>

These characteristics make it a powerful instrument for determining the composition and mapping of an asteroid's surface with an average spectral sampling of 1.8 nm/band in the visible (VIS) and 9.8 nm/band in the infrared (IR). The spatial sampling may vary from a few kilometers/pixel to a few tens meters/pixel, depending on the altitude of the spacecraft over the surface.<sup>3</sup> VIR characteristics are summarized in Table I. The mission was divided into different main phases on the basis of the spacecraft altitude: Approach, Rotation

Characterization (RC), both before gravitational capture and orbiting of Dawn, then the orbital phases Survey, High-Altitude Mapping Orbit (HAMO), and Low-Altitude Mapping Orbit (LAMO). Each phase is different from the others in terms of duration, illumination conditions, and altitude over the surface, decreasing from Approach to LAMO (Fig. 2).

A spectrometer typically consists of an optical head, an entrance slit, a dispersing element (such as a grating), and a detector. VIR combines two push-broom channels of 256 spatial pixels by 432 spectral pixels operating in the 0.25–1.05  $\mu\text{m}$  (VIS channel) and in the 1.0–5.1  $\mu\text{m}$  (IR channel) spectral domains. In this design, sunlight reflected from the target, after passing through a slit, is dispersed by a grating onto a 2-dimensional detector array (a CCD for the VIS channel and a HgCdTe array for the IR channel). Because of the inclusion of a dispersing element, the spatial image of the entrance slit falls on different regions of the detector array, depending on its wavelength.<sup>3</sup> The columns of the array are parallel to the slit, and thus the spectral information is dispersed along the rows of the detector. VIR data are hyperspectral images (“cubes”), i.e., 3D arrays (Fig. 3), with two spatial dimensions (sample, line) and one spectral dimension (band).

One advantage of this technique is that each pixel inside the hyperspectral image has a spectrum in the overall range 0.25–5.1  $\mu\text{m}$ , showing the intensity of light at each wavelength for that specific location. Alternatively, it is possible to select a specific wavelength and extract a monochromatic image for that specific wavelength.<sup>3</sup>

The quality of the calibration is important for identifying surface materials. An imperfect calibration could distort an

<sup>a)</sup>giacomo.carrozzo@iaps.inaf.it



FIG. 1. VIR optical head during the last phases of integration and test at Finmeccanica (credit Finmeccanica).

absorption feature, causing a misidentification. An accurate calibration makes the data adequate to study the properties of surface materials and is a key in linking remotely sensed surface properties with laboratory data.<sup>4</sup> After the radiometric calibration, imaging spectrometers are often still affected by other sources of systematic errors. These residual errors may affect the identification, and physical and mineral characterization of surface materials.<sup>4</sup> For this reason, identifying and correcting data artifacts are important for a proper interpretation of the spectra. Various authors describe algorithms for artifacts removal for an imaging spectrometer [e.g., Refs. 5–7].

Data acquired by the VIR spectrometer are systematically affected by artifacts, vertical stripes, and spikes. In VIR data, they are caused by imperfect radiometric and spectral calibration. The goal of our work is to identify systematic artifacts and develop a de-noising algorithm. We test this spectral polishing technique in order to remove artifacts from

TABLE I. VIR main characteristics.

VIR main characteristics			
		VIR VIS channel	VIR IR channel
Spectral performances	Spectral range	0.25–1.05	1.0–5.0
	Spectral sampling (high resolution)	1.08 nm/band (432 bands)	9.8 nm/band (432 bands)
	Spectral resolution $\lambda/\Delta\lambda$	100–380	70–360
Spatial performances	IFOV (high resolution)	250 × 250 mrad	
	FOV (high resolution)	64 × 64 mrad	
Mass		20 kg	
Telescope	Pupil diameter	27.1 mm	47.5 mm
	Focal length	152 mm	

VIR data. We also show comparisons of images and spectra before and after the application of this algorithm to both the mission targets, Vesta and Ceres.

## II. CALIBRATION AND MINIMIZATION OF SPECTRAL ARTIFACTS

The calibration pipeline allows the conversion of the signal from raw digital numbers to physical units of spectral radiance.<sup>8</sup> To achieve that, we derived the spectral response function of the instrument using the measurements made during the on-ground calibration campaign.<sup>3</sup> The calibration pipeline computes the radiance from the raw signal, including a correction for the instrumental thermal background. For details, see the work of Filacchione and Ammannito.<sup>9</sup> At the end, radiance is divided by solar spectrum to obtain a calibrated radiance factor ( $I/F$ ) using the formulation,

$$I/F = \frac{\pi \cdot I}{F_s \cdot d^2},$$

where  $F_s$  is the solar flux (irradiance) at 1 astronomical unit (AU),  $I$  is the calibrated radiance ( $\text{W} \cdot \text{m}^{-2} \mu\text{m}^{-1} \text{sr}^{-1}$ ) measured

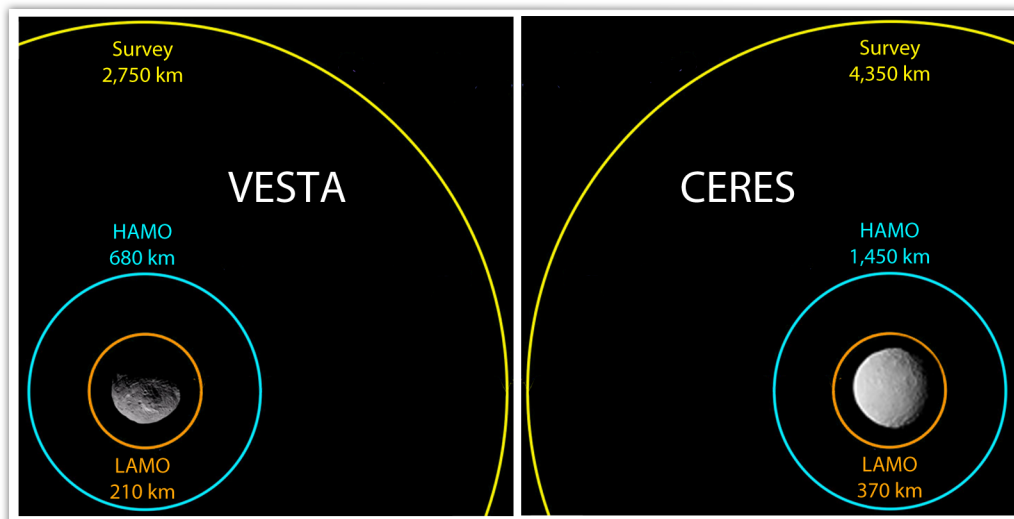


FIG. 2. Different main mission phases for Vesta and Ceres (the orbits here are only approximate) with the distance from the surface of the target.

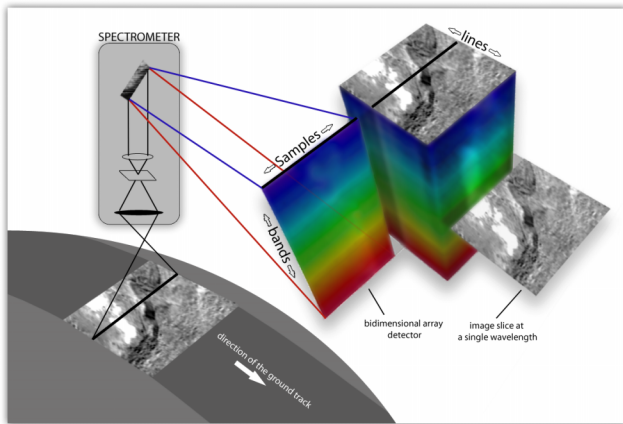


FIG. 3. The readout of each detector is one line of a spatial image containing the spectral information. The whole image is built as a DAWN spacecraft (and thus the VIR spectrometer) moves along its ground track or using the internal scanning mirror.

by the VIR instrument, and  $d$  is the heliocentric distance of the target (Vesta or Ceres) expressed in AU.

During the mission operations at Vesta, we have identified some artifacts in the instrumental response function (IRF) in the 2.5–3.5  $\mu\text{m}$  spectral range, where several absorption bands of OH and H<sub>2</sub>O occur. These artifacts are systematic, and therefore they did not prevent the detection of relative spectral variations associated with OH and H<sub>2</sub>O, if any. These artifacts are systematic errors due to the non-homogenous

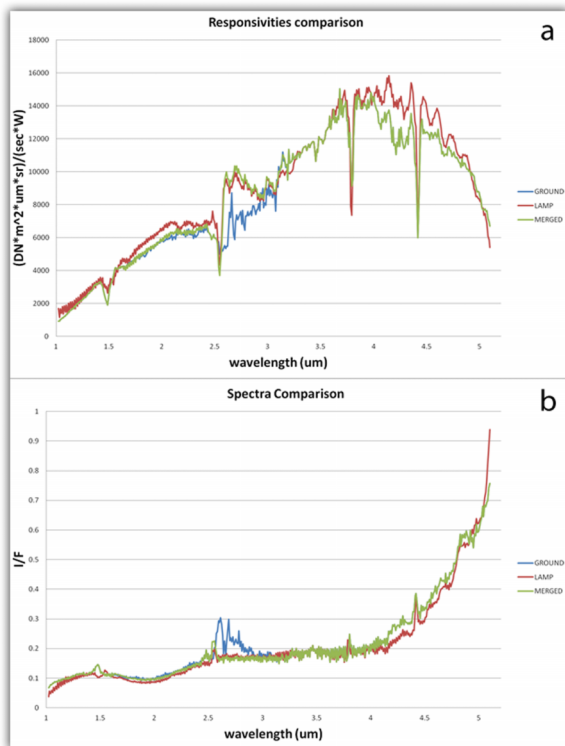


FIG. 4. Comparison among (a) the instrumental response function obtained with the on-ground calibration (blue curve) with the in-flight calibration (red curve) and a combination of the two (green curve) and (b) the calibrated spectra computed with these three versions of the instrumental response function.

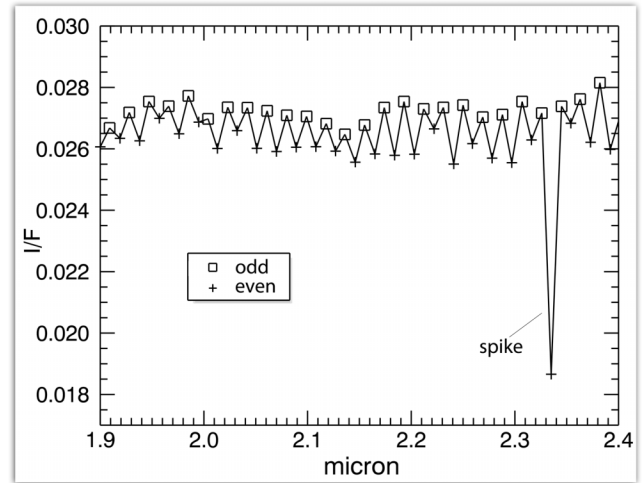


FIG. 5. Details of a generic VIR spectrum in the IR spectral domain. It is evident the odd and even effect, and the presence of a spike.

instrumental response of a detector producing nonphysical spectral signatures. They are caused by imperfect radiance calibration, by spectral miscalibration, by a peculiar readout noise in the detector electronics, and from uncertainties in the solar reference spectrum.<sup>5</sup>

### A. Standard calibration

The first paper published in which spectra in this range are discussed<sup>10</sup> used a different calibration method described in the paper itself. This method used a simple correction of the IRF based on an empirical calibration correction that is appropriate to recover the signal in that specific range. However, the absolute absorption band depth in this range could not be calculated. To compute the IRF for this range, we used one of the internal lamps of the spectrometer. This lamp, made of a tungsten filament, is characterized by a blackbody-like emission at about 2400 K.<sup>11</sup> Since the spectrum of the infrared radiation emitted by these filaments is featureless, a polystyrene filter was inserted for a wavelength calibration of the IR channel. The blackbody radiation of the internal lamp has been used to retrieve a relative IRF in the 2.5–3.5  $\mu\text{m}$  spectral range.

First, we calibrated the signal from the internal calibration lamp with the on-ground response function, and then we retrieved the equivalent temperature of the radiation fitting a Planck curve. The new IRF is the result of the ratio between the raw signal of the lamp and the Planck function. This

TABLE II. Ranges of the order-sorting filter junctions where there is a loss of linearity. In Figures 8 and 9, these spectral regions are shown in dark gray areas.

Filter junctions	
VIR-VIS channel	$0.67 \mu\text{m} < \lambda < 0.68 \mu\text{m}$
	$1.42 \mu\text{m} < \lambda < 1.56 \mu\text{m}$
	$2.41 \mu\text{m} < \lambda < 2.61 \mu\text{m}$
VIR-IR channel	$3.74 \mu\text{m} < \lambda < 3.83 \mu\text{m}$
	$4.35 \mu\text{m} < \lambda < 4.54 \mu\text{m}$

ratio must be multiplied by a factor to take into account the integration time used to acquire the signal, the transmittance of the polystyrene filter, and the viewing geometry. We compared the IRF (Fig. 4(a)) obtained with the on-ground calibration (blue curve) with the in-flight calibration (red curve) and a combination of the two (green curve), and we analyzed the calibrated spectra computed with these three versions of the IRF (Fig. 4(b)). We observe that the new IRF minimizes most calibration residuals that were showing as artifact peaks between 2.5 and 2.9  $\mu\text{m}$  in the previous calibration. The adopted IRF (downloadable from PDS website as V2) is the IRF derived during the on-ground calibration campaign with the exception of the spectral channels between 2.5 and 3.5  $\mu\text{m}$  where the IRF derived using the method described here has been used.

## B. Artifacts

The spectra calibrated with the standard data reduction procedure described in the previous paragraph are affected by some spurious effects observed in the spectral and spatial dimensions. Given their different origin and structure, we developed a method to minimize the different types of artifacts that we have identified.

### 1. Odd-even band effect in the spectra

VIR-IR spectra present a saw-tooth pattern that is associated with the odd and even band (wavelength) numbers (Fig. 5). This is a common problem found into detectors. The signal is read by a pair of bi-dimensional array of IR-sensitive photo-voltaic mercury cadmium telluride coupled to the silicon CMOS multiplexers.<sup>3</sup> Each multiplexer is configured to read the odd and even signal of the detector columns (i.e., the bands), and their different electronic offset in the readout results in the spectral pattern as in Fig. 5. We

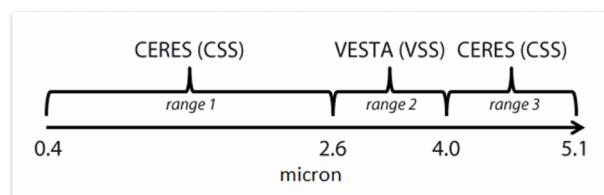


FIG. 6. Mission phases used in the spectral ranges to compute the artifact matrix. VSS = Survey mission phase for Vesta and CSS = Survey mission phase for Ceres.

assume that the signal in output is proportional to the flux of photons hitting the detector.

### 2. Spectral spikes

Spectral spikes are random anomalies involving one or a limited set of detector pixels (Fig. 5). Usually they are pixels where an anomalous variation of the signal is present due to random events (for example, a cosmic ray hitting the detector). They are detectable as outliers in the overall statistics of the signal. These spikes are clearly not related to the mineralogy and an algorithm was implemented to remove them. VIR data show also spatial stripes. They can be observed as an aligned pattern crossing the whole images (different for each wavelength) and are due to the slight variation in the overall instrumental transfer function among different samples of the detector.

### 3. Vertical stripes in the images

Along-track stripes are clearly visible through as a vertical (along lines) pattern on the whole image at a given wavelength. In general, the standard calibration is effective in removing stripes as long as they are a multiplicative perturbation of the

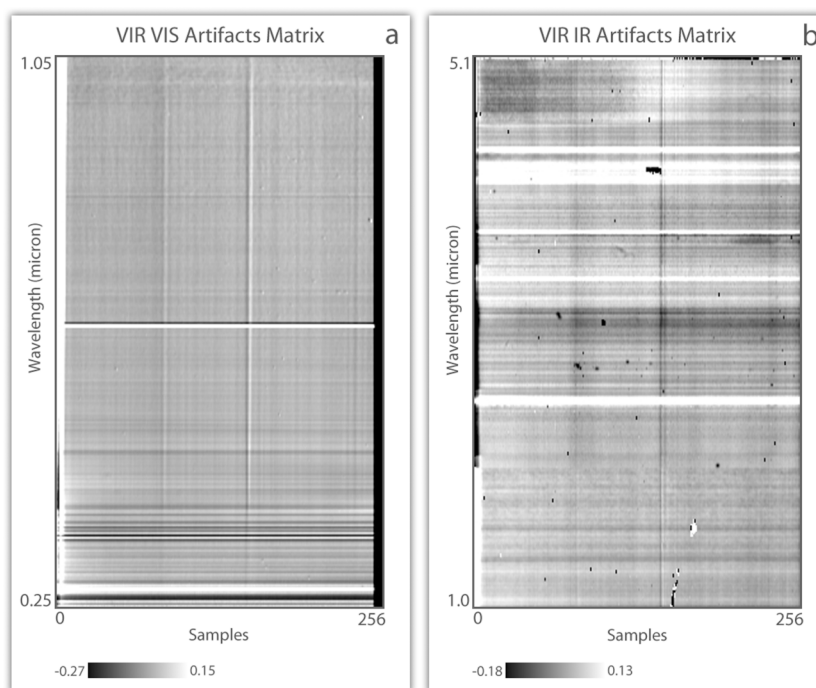


FIG. 7. For (a) visible and (b) infrared VIR artifacts matrix.

signal. However, residual uncorrected stripes pattern can still exist probably due to an additive perturbation of the signal. The stripes can be one or more pixels wide and can be brighter or darker than adjacent lines<sup>12</sup> and their relative intensity may also vary across the image. Moreover, they are similar in VIR datasets acquired at different parts of the mission. This systematic character indicates that the stripes are due to differences in the relative response of the sample detectors, but they are not due to any instability in the instrument. The variation of sensibility among the detector elements is usually corrected by means of flat fielding, which is of course different for the two VIR detectors.

#### 4. Artifacts

Variations at a small spectral scale can occur systematically due to the non-homogenous instrumental response of the detector. They can influence the quality of the spectra producing nonphysical spectral signatures that might be interpreted as representing a material that does not really exist at that location.

#### C. Artifact minimization

The de-noising procedure presented here is an adaptation to VIR/Dawn data of the method used for the artifact reduction of VIRTIS/Rosetta data<sup>7</sup> which proved to be effective in minimizing spectral artifacts and retrieve the signal coming from the target. Our algorithm is not the same used for VIRTIS dataset. The concept is similar but our routine is completely rewritten *ad hoc* for VIR data. It is worth noting that the algorithm is unable to correct the spectra in correspondence with the junction of the grating order filters (see Table II for details) and in the 1.02–1.05  $\mu\text{m}$  spectral ranges because of the loss of linearity, and between 0.25 and 0.4  $\mu\text{m}$  because of low sensitivity of the instrument.<sup>3</sup>

We developed a correction of artifacts in a two steps process: (1) creation of the artifacts matrix and (2) application of the artifacts matrix to the VIR cubes. In VIR data, detector artifacts change from sample to sample (column dependency). In the approach presented here, a polynomial function is used to fit the high frequency variations. In order to study these effects, the dataset used includes the following:

- VIR data acquired in the Survey mission phase at Ceres (CSS) to compute the artifact profiles in the VIS channel.
- VIR data acquired in the Survey mission phases at Ceres and Vesta (CSS and VSS) to compute the artifact profiles in the IR channel.

To compute the artifact profiles, we use the mission phases and the spectral ranges where there are no relevant absorptions. Starting from this dataset, we obtain a median spectrum that characterizes systematic residuals for each sample.

##### 1. Creation of the artifacts matrix

The algorithm consists of the following sub-steps:

- For each sample, about 20 000 reflectance spectra are selected using data acquired in the Survey mission phase

at Ceres (in the VIS channel from 0.4 to 1.02  $\mu\text{m}$  and in the IR channel from 1.02 to 2.59  $\mu\text{m}$  [range 1] and from 4.07 to 5.1  $\mu\text{m}$  [range 3]) and using data acquired in the Survey mission phase at Vesta (in the IR channel from 2.59 to 4.07  $\mu\text{m}$  [range 2]). Choosing different targets (Vesta and Ceres) in different wavelength ranges (Fig. 6) helps us exclude those spectral ranges affected by relevant absorption features, which could affect the polynomial fit used to characterize the high frequency artifacts. Using the shape model of Ceres, we use the local condition of insolation to exclude all spectra with solar incidence angles larger than 60°, i.e., affected by grazing sunlight.

- For each sample, a median spectrum  $S_{med}(s, \lambda)$  is computed. In other words, we took the median signal of all pixels of a given wavelength for the entire VIR dataset.
- For each  $S_{med}(s, \lambda)$ , the odd and even effect due to the electronic offset is removed by means of interpolation (Fig. 5). The correction for a given channel is performed

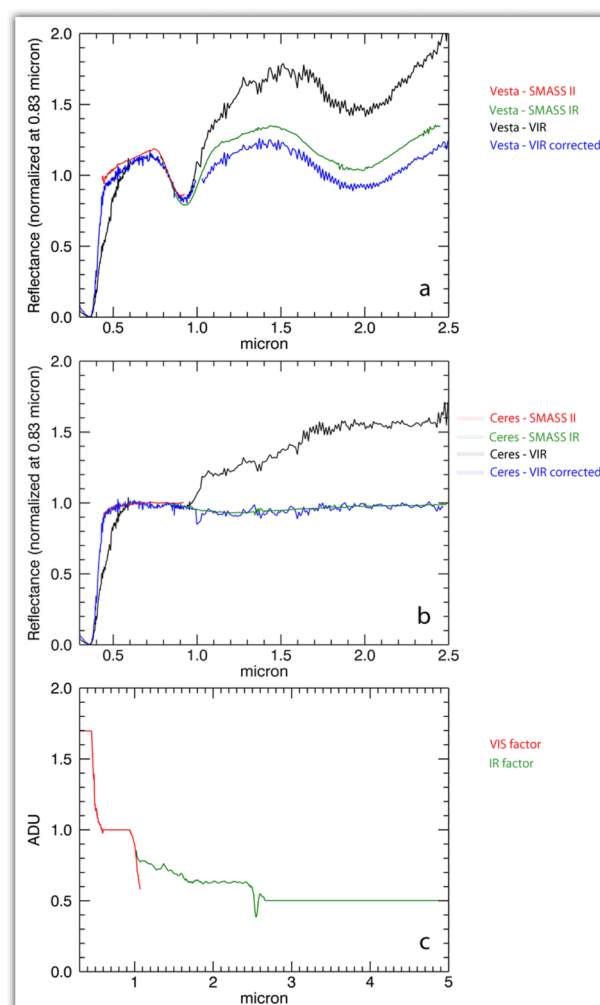


FIG. 8. For Vesta (a) and Ceres (b), respectively, it is shown the SMASS\_II spectrum (red color), the SMASS\_IR spectrum (green color), a generic spectrum (black curve), and the same spectrum corrected multiplied for the ground factor correction. (c) Correction factor applied to the VIR spectra: SMASS\_II covers the range 0.43–0.925  $\mu\text{m}$  (red color), while SMASS\_IR covers 0.8–2.5  $\mu\text{m}$  (green color). All spectra normalized at 0.83  $\mu\text{m}$ .

by calculating a weighted averaged of its value with those of the two neighboring channels.<sup>13</sup>

4. For each  $S_{med}(s, \lambda)$ , a standard despiking procedure is applied to remove random spikes. These spikes are identified by applying a 3- $\sigma$  threshold to the ratio between a spectrum and its running average over 3 spectral points. The values identified as spikes are then substituted with a 2nd degree polynomial function fitting the 20 neighboring bands (Fig. 5).
5. A unique median spectrum  $U_{med}(\lambda)$  is obtained by computing the median of  $S_{med}(s, \lambda)$  over the samples.
6. A polynomial function  $P_U(\lambda)$  is fitted to  $U_{med}(\lambda)$ .
7. For each sample, the artifacts matrix is defined as

$$A(s, \lambda) = \frac{S_{med}(s, \lambda) - P_U(\lambda)}{P_U(\lambda)}.$$

The output of this procedure is a 2D-matrix [number of samples, number of wavelengths] hereafter called “artifacts matrix” or  $A(s, \lambda)$ . Such a matrix represents the residual of the spectrum extracted from each sample has with respect to the average (Fig. 7).

## 2. Application of the artifacts matrix to the VIR cubes

In the last step, we remove the column-dependent artifacts from the reflectance values applying the artifacts matrix to the VIR reflectance spectra for each line, similarly to a flat-field correction:

1. For each spectrum, the odd and even effects due to the electronic offset are removed with an interpolation using the same method of point 3.
2. For each line  $l$ , the new VIR spectra  $R'(s, l, \lambda)$  are computed as follows:

$$R'(s, l, \lambda) = \frac{R(s, l, \lambda)}{1 + A(s, \lambda)},$$

where  $R(s, l, \lambda)$  are the VIR spectra at the line  $l$ , which is a 2D-matrix [number of samples, number of wavelengths].

After the artifact removal is applied, residual vertical stripes may still exist. Any spectral parameter involving band ratios, for example, may enhance such calibration residuals. Therefore, for more complete minimization of artifacts in the

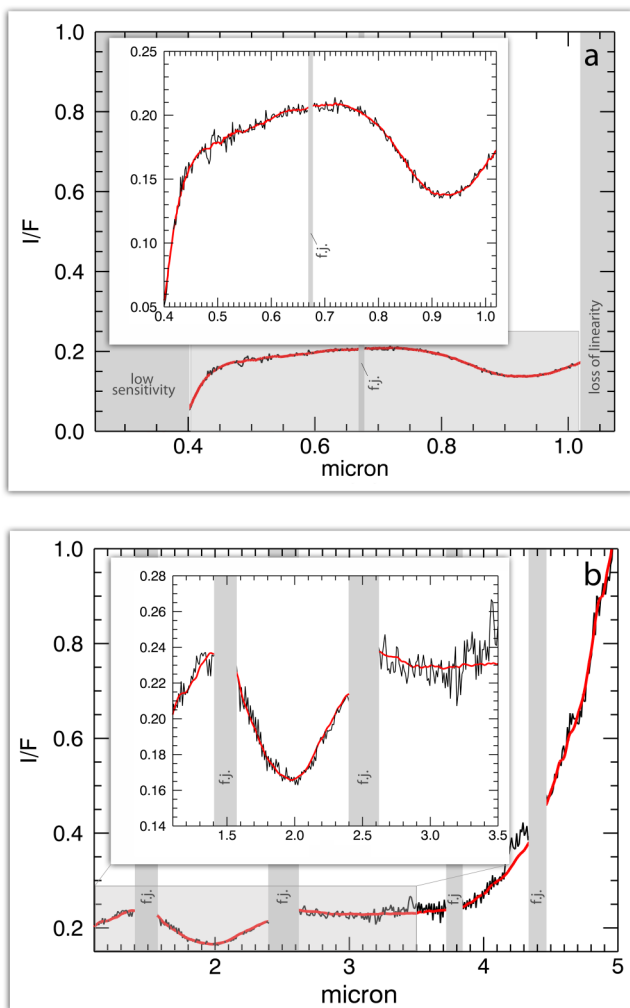


FIG. 9. (a) Typical VIR-VIS and (b) VIR-IR reflectance spectrum of Vesta (black) and the same one after the artifacts have been removed (red). In order to illustrate finer details, a portion of the spectrum is shown in the inset. The dark gray areas show the spectral regions with loss of linearity (e.g., the filter junctions named f.j.), and those with low sensitivity.

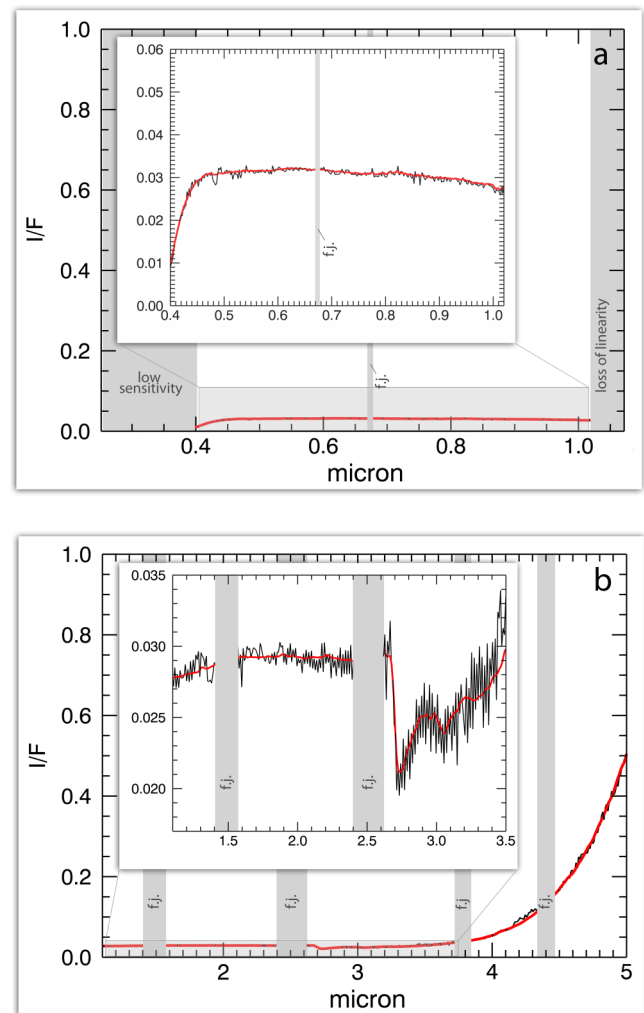


FIG. 10. (a) Typical VIR-VIS and (b) VIR-IR reflectance spectrum of Ceres (black) and the same one after the artifacts have been removed (red). To get more details, a portion of the spectrum is shown in the inset. The dark gray areas show the spectral regions with loss of linearity (e.g., the filters junction named f.j.), and those with low sensitivity.

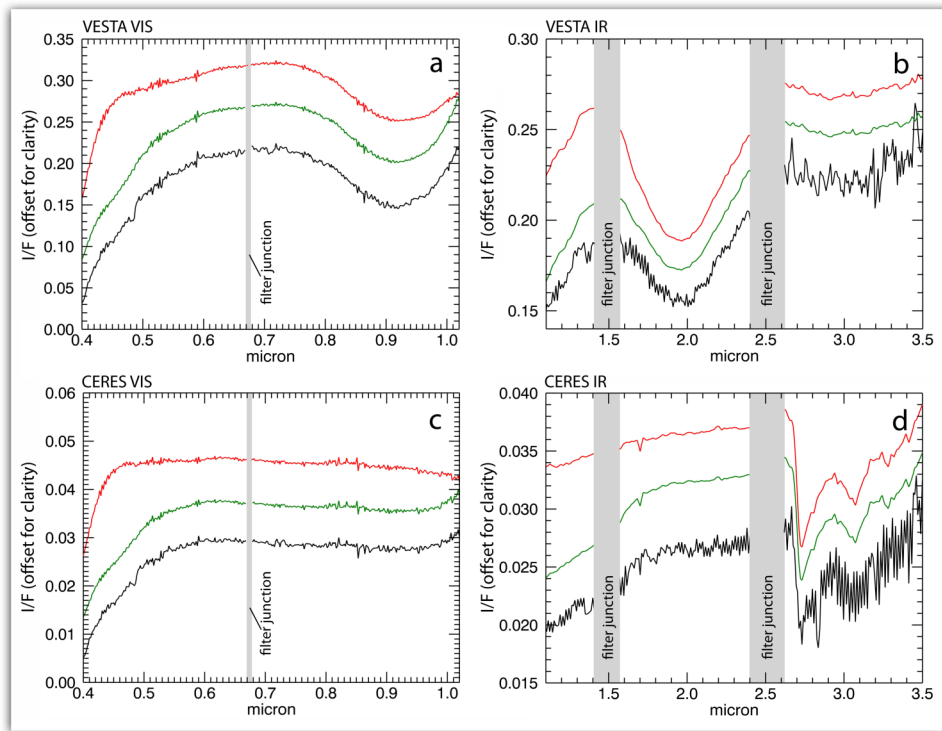


FIG. 11. Comparison of a generic reflectance spectrum of Vesta ((a) and (b)) and Ceres ((c) and (d)) before the new calibration (black curves), after the new calibration (green curves), and after the ground correction factor has been applied to the new calibration (red curves).

data, further corrections such as offsets may be calculated and be specifically adapted. In order to remove this component, further corrections must be applied by means of an additive algorithm. A routine for the removal of these residual vertical stripes is currently under study and will be implemented in future releases.

#### D. Ground correction

Since VIR spectra are affected by a positive slope in the VIS-NIR range when compared to ground based spectra of the same target (Vesta and Ceres), we decided to re-normalize VIR dataset to correct this effect. The origin of this slope effect is not currently understood.

The correction is a scale factor computed as the ratio between a ground based reference and VIR spectrum of Ceres, both normalized at 550 nm.

The ground based reference used is the combination of SMASS\_II<sup>14</sup> and SMASS\_IR.<sup>15</sup> These spectra have been merged and interpolated to VIR spectral sampling. The VIR spectrum used is the average of all the spectra with a phase angle lower than 25° in the RC3 mission phase.<sup>16</sup> For a proper calibration, the VIR spectra have to be multiplied for this factor (Fig. 8).

### III. RESULTS

The algorithm described here was tested for both the VIR datasets obtained at both Vesta and Ceres. Its application results in greatly improved quality of hyperspectral images by minimizing artifacts, and flat-field and stripes biases. Figures 9

and 10 show the result for a generic spectrum of Vesta and Ceres, respectively. In both cases, the same spectrum is shown as calibrated using the standard pipeline (Sec. II A) and processed using the described method (Secs. II B and II C).

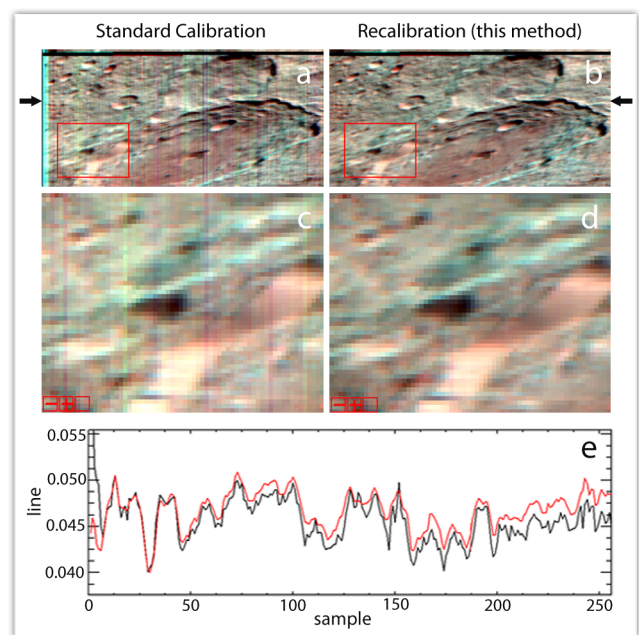


FIG. 12. Cube 498 058 497 in RGB ( $R=1.34 \mu\text{m}$ ;  $G=2.01 \mu\text{m}$ ;  $B=4.02 \mu\text{m}$ ) before ((a) and (c)) and after ((b) and (d)) the recalibration procedure. (c) and (d) are a close-up of (a) and (b), respectively (see red boxes in (a) and (b)). (e) shows the horizontal profile at  $2.01 \mu\text{m}$  along the line indicated by the arrow in order to show the effect of the artifacts removal (black curve: standard calibration, red curve: recalibration).

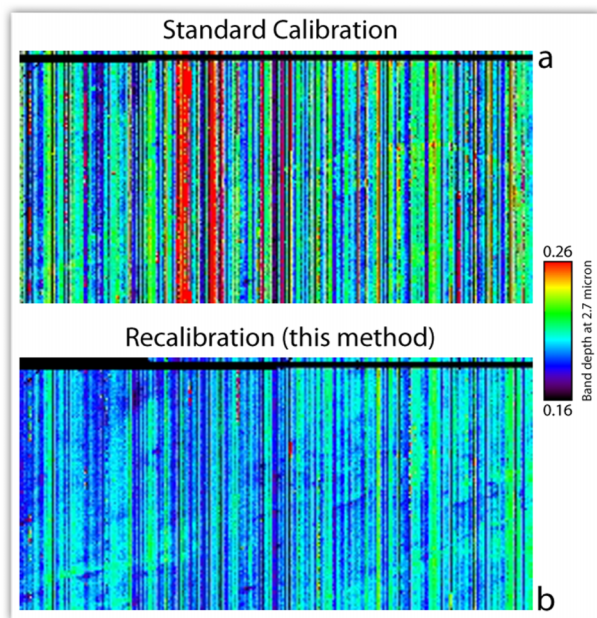


FIG. 13. Band depth at  $2.7\ \mu\text{m}$  computed for the cube 498 058 497 using the standard calibration (a) and after the recalibration procedure (b).

After the artifact reduction, absorption bands (if present) are more evident, enabling an easier determination of the band minimum and band center. This is clear in Figure 10(b) where, after artifacts removal, absorption at  $\sim 3.3\ \mu\text{m}$  is more evident in agreement with the observations from the ground.<sup>17</sup>

In order to emphasize the difference between the main steps of the calibration, a plot showing spectra with standard ITF, new ITF, and new ITF + ground correction is shown in Figure 11. The comparison among these spectra shows different spectral slopes. This is particularly evident in the case of Vesta where the shape of the broad absorption feature centered about  $1\ \mu\text{m}$  (due to crystal-field transitions of  $\text{Fe}^{2+}$  ions) is affected by the new calibration.

The artifacts correction works also as an additional flat field correction. The resulting improvement of the image quality can be noticed in Figures 12 and 13. It is worth noting that, although strongly reduced, a light stripes pattern is still perceivable in the corrected images. A specific procedure is needed to remove such fine structures, which is not discussed in this work.

In the light of these results, the method has been applied to the entire VIR dataset. In this paper we show the importance of spectral de-noising in the calibration pipeline. The described algorithm is suitable for other, present and future, imaging spectrometers.

The VIR de-noised IR dataset is currently under publication, and the complete Ceres Campaign including the LAMO (Low Altitude Mapping Orbit) phase will be publicly available on NASA Planetary Data System by the beginning of the next year. The planned release includes the full corrected data set (both Vesta and Ceres) and it implements the described procedure.

## ACKNOWLEDGMENTS

We thank the Italian Space Agency (ASI). The VIR instrument was funded and coordinated by the ASI and built by Selex ES, with the scientific leadership of the Institute for Space Astrophysics and Planetology, Italian National Institute for Astrophysics, Italy, and it is operated by the Institute for Space Astrophysics and Planetology, Rome, Italy.

- <sup>1</sup>C. T. Russel *et al.*, “Exploring the asteroid belt with ion propulsion: Dawn mission history, status and plans,” *Adv. Space Res.* **40**(2), 193–201 (2007).
- <sup>2</sup>C. T. Russel *et al.*, “Dawn at vesta: Testing the protoplanetary paradigm,” *Science* **336**(6082), 684–686 (2012).
- <sup>3</sup>M. C. De Sanctis *et al.*, “The VIR spectrometer,” *Space Sci. Rev.* **163**, 329–369 (2011).
- <sup>4</sup>R. N. Clark *et al.*, “Surface reflectance calibration of terrestrial imaging spectroscopy data: A tutorial using AVIRIS,” in *Proceedings of the 10th Airborne Earth Science Workshop* (JPL Publication, 2002), Vol. 02(1).
- <sup>5</sup>D. Schlöpfer and R. Richter, “Spectral polishing of high resolution imaging spectroscopy data,” in *presented at 7th SIG-IS Workshop on Imaging Spectroscopy, Edinburgh* (Edinburgh Publication, 2011), p. 7.
- <sup>6</sup>M. Parente, “A new approach to denoising CRISM images,” presented at 39th LPSC, abstract #2528, 2008.
- <sup>7</sup>A. Raponi, “Spectrophotometric analysis of cometary nuclei from *in situ* observations,” Ph.D. dissertation (Università degli studi di Roma Tor Vergata, 2014).
- <sup>8</sup>A. Coradini *et al.*, “VIR-visual infrared mapping spectrometer of dawn mission,” 39th LPSC, #1556, 2008.
- <sup>9</sup>G. Filacchione and E. Ammannito, Dawn VIR Calibration Document, version 2.4, [http://sbn.psi.edu/archive/Dawn/vir/DWNVVIR\\_I1B/DOCUMENT/VIR\\_CALIBRATION/VIR\\_CALIBRATION\\_V2\\_4.PDF](http://sbn.psi.edu/archive/Dawn/vir/DWNVVIR_I1B/DOCUMENT/VIR_CALIBRATION/VIR_CALIBRATION_V2_4.PDF), 2014.
- <sup>10</sup>M. C. De Sanctis *et al.*, *ApJL* **758**, L36 (2012).
- <sup>11</sup>R. Melchiorri *et al.*, *Rev. Sci. Instrum.* **74**(8), 3796–3801 (2003).
- <sup>12</sup>C. Weiwei *et al.*, “A study on destriping methods of imaging spectrometer images,” in *The Eighth International Conference on Electronic Measurement and Instruments* (IEEE, 2007), pp. 2766–2771.
- <sup>13</sup>J.-P. Combe *et al.*, “Reflectance properties and hydrated material distribution on vesta: Global investigation of variations and their relationship using improved calibration of dawn VIR mapping spectrometer,” *Icarus* **259**, 21–38 (2015).
- <sup>14</sup>S. J. Bus and R. P. Binzel, “Phase II of the small main-belt asteroid spectroscopic survey: The observations,” *Icarus* **158**, 106–145 (2002).
- <sup>15</sup>T. H. Burbine and R. P. Binzel, “Small main-belt asteroid spectroscopic survey in the infrared,” *Icarus* **159**, 468–499 (2002).
- <sup>16</sup>M. C. De Sanctis *et al.*, Dawn VIR CAL (RDR) Ceres Infrared Spectra V1.0, DAWN-A-VIR-3-RDR-IR-CERES-SPECTRA-V1.0, NASA Planetary Data System, 2015.
- <sup>17</sup>A. S. Rivkin *et al.*, “The surface composition of ceres,” *Space Sci. Rev.* **116**, 163–195 (2011).